



**HAL**  
open science

# Rovibrational laser jet-cooled spectroscopy of the NH<sub>3</sub> –Ar complex in the $\nu$ 2 umbrella region of NH<sub>3</sub>: comparison between new infrared data and an ab initio calculated spectrum

Pierre Asselin, Yacine Belkhodja, Atef Jabri, Alexey Potapov, Jérôme Loreau, Ad van Der Avoird

## ► To cite this version:

Pierre Asselin, Yacine Belkhodja, Atef Jabri, Alexey Potapov, Jérôme Loreau, et al.. Rovibrational laser jet-cooled spectroscopy of the NH<sub>3</sub> –Ar complex in the  $\nu$  2 umbrella region of NH<sub>3</sub>: comparison between new infrared data and an ab initio calculated spectrum. *Molecular Physics*, 2018, 116 (23-24), pp.3642 - 3655. 10.1080/00268976.2018.1471533 . hal-01912258

**HAL Id: hal-01912258**

**<https://hal.sorbonne-universite.fr/hal-01912258>**

Submitted on 13 Nov 2018

**HAL** is a multi-disciplinary open access archive for the deposit and dissemination of scientific research documents, whether they are published or not. The documents may come from teaching and research institutions in France or abroad, or from public or private research centers.

L'archive ouverte pluridisciplinaire **HAL**, est destinée au dépôt et à la diffusion de documents scientifiques de niveau recherche, publiés ou non, émanant des établissements d'enseignement et de recherche français ou étrangers, des laboratoires publics ou privés.

**Rovibrational laser jet-cooled spectroscopy  
of the NH<sub>3</sub>-Ar complex in the  $\nu_2$  umbrella region of NH<sub>3</sub> :  
comparison between new infrared data and an *ab initio* calculated spectrum**

P. Asselin<sup>a</sup>, Y. Belkhouja<sup>a</sup>, A. Jabri<sup>a</sup>, A. Potapov<sup>b</sup>, J. Loreau<sup>c</sup> and A. van der Avoird<sup>d</sup>

<sup>a</sup>Sorbonne Université, CNRS, MONARIS, UMR 8233, 4 place Jussieu, Paris, F-75005 France.

<sup>b</sup>Laboratory Astrophysics Group of the Max Planck Institute for Astronomy at the Friedrich Schiller University Jena, Germany.

<sup>c</sup>Service de Chimie Quantique et Photophysique, Université libre de Bruxelles (ULB) CP 160/09, 50 av. F.D. Roosevelt, 1050 Brussels, Belgium.

<sup>d</sup>Theoretical Chemistry, Institute for Molecules and Materials, Radboud University Nijmegen, Heyendaalseweg 135, 6525 AJ Nijmegen, The Netherlands.

## Abstract

Five ortho and para bands of the  $\nu_2$  umbrella mode of the NH<sub>3</sub>-Ar van der Waals complex have been recorded at high resolution using jet-cooled infrared laser spectroscopy. A rovibrational analysis provides accurate band centers and upper state rotational constants for the  $\Pi_s(j=1, k=0) \leftarrow \Sigma_a(j, k=0)$  and  $\Sigma_s(j=1, k=0) \leftarrow \Sigma_a(j, k=0)$  ortho bands. The puzzling para bands observed in the region of the lower and upper components of the inversion splitting doublet have been assigned by comparison with rovibrational and tunneling levels and transitions calculated *ab initio*. The latter calculations are based on the four-dimensional potential energy surface reported by Loreau et al. [J. Chem. Phys. **141**, 224303 (2014)], which takes explicitly into account the umbrella motion of the ammonia molecule. The very good agreement found between  $\Pi_{s/a, \text{lower}}(j=1, k=1) \leftarrow \Sigma_a(j=1, k=1)$  and  $\Pi_{s/a, \text{upper}}(j=1, k=1) \leftarrow \Sigma_s(j=1, k=1)$  experimental and calculated transitions has been exploited to determine precisely two different inversion splittings in the  $\nu_2$  state (32.003(1) and 36.008(1) cm<sup>-1</sup>) from extrapolated Q(0) line frequencies and to obtain a qualitative picture of Coriolis couplings present in both the  $\nu_2=0$  and  $\nu_2=1$  states.

## Introduction

The interaction of ammonia with rare gases has been the subject of a large number of studies motivated mainly by the interest in weak interactions<sup>1</sup> and, in particular, in the effect of the van der Waals (vdW) interaction on the NH<sub>3</sub> inversion tunneling. The inversion-tunneling splitting in NH<sub>3</sub> is extremely sensitive to intermolecular interactions and thus represents a valuable probe of asymmetry in the intermolecular potential energy surface (PES) and the vibration-rotation-tunneling (VRT) states of NH<sub>3</sub> complexes along the inversion coordinate. Upon complexation, NH<sub>3</sub> generally acts as a hydrogen acceptor and binds (near) axially to its binding partner.<sup>2</sup> This leads to a large asymmetry in the NH<sub>3</sub> inversion potential which quenches the tunneling, but NH<sub>3</sub>-Ar has been considered as an exception to this case.

The NH<sub>3</sub>-Ar vdW complex has been the subject of extensive microwave and far infrared spectroscopic studies. The first measurements were performed in the microwave region.<sup>3,4</sup> They determined the expectation value of the intermolecular separation, the dipole moment and the nuclear quadrupole coupling constant. In addition to the assigned pure rotational transitions, many other transitions due to the non-rigidity of the complex were observed and attributed to inversion-tunneling transitions<sup>5,6,7,8,9</sup>, which showed that ammonia behaves almost as a free rotor in the complex. This large collection of results provided further evidence for the free-rotor picture from the precise knowledge of the bound states of the complex, that correlate to the  $j_k = 0_0, 1_0$  and  $1_1$  levels of free NH<sub>3</sub>, including states with vibrational excitations in the vdW stretching coordinate.

Early *ab initio* studies combined with these in-depth far-infrared measurements led to a semi-empirical intermolecular PES obtained by fitting the experimental data.<sup>10</sup> Structures with various possible orientations of ammonia relative to the vdW bond axis were found, depending on whether the internal angular momentum of the almost freely rotating NH<sub>3</sub> unit, is roughly directed along ( $\Pi$ ) or perpendicular ( $\Sigma$ ) to this axis.<sup>7,8</sup>

Several more and more sophisticated PESs have been developed over the years to improve the understanding of spectroscopic data. More recently, good agreement was obtained between geometry optimizations performed by Bistoni et al.<sup>11</sup> using the coupled cluster method, and molecular beam experiments probing the isotropic part of the PES. In 2014, a four-dimensional (4D) PES was computed by Loreau et al.<sup>12</sup> that includes explicitly the  $\nu_2$  umbrella motion of NH<sub>3</sub> and ND<sub>3</sub>. Further insight into the internal-rotation dynamics of the complex could be obtained from a direct comparison between the bound states of both NH<sub>3</sub>-Ar and ND<sub>3</sub>-Ar calculated on this PES for total angular momentum values up to  $J = 10$  with the inclusion of Coriolis interactions, and spectroscopic data accumulated over 30 years in the microwave and far-infrared regions for both complexes.

Mid-<sup>13,14</sup> and near-infrared<sup>15</sup> data on NH<sub>3</sub>-Ar remain scarce due to the lack of broadband laser sources in both regions. Using a microwave-sideband CO<sub>2</sub> laser optothermal spectrometer, Fraser et al.<sup>13</sup> observed a  $\Pi \leftarrow \Sigma$  type infrared transition in the  $\nu_2$  umbrella excited state and derived spectroscopic constants containing information about the  $\nu_2$  dependence of the NH<sub>3</sub>-Ar interaction. From the microwave-infrared double-resonance technique, Fraser et al.<sup>13</sup> and Bizzari et al.<sup>14</sup> also found in the same region three CO<sub>2</sub> laser coincidences, respectively at 938.6893, 970.5498 and 974.6248 cm<sup>-1</sup>. The observation of two high frequency rovibrational lines, located 32 and 36 cm<sup>-1</sup> above the transition of Fraser et al.<sup>13</sup> was taken as further evidence that the NH<sub>3</sub> inversion frequency is essentially unchanged upon complexation, since the tunneling splitting in  $\nu_2=1$  for free NH<sub>3</sub> is about 36 cm<sup>-1</sup>.

In the present paper, we describe high resolution infrared laser jet-cooled measurements in the  $\nu_2$  umbrella mode region of NH<sub>3</sub>-Ar. The main objective is to provide new reliable infrared data to be compared with VRT levels of the ground and  $\nu_2=1$  excited state calculated on the 4D PES of Loreau et al.<sup>12</sup>, the most advanced

one computed so far, and thereby to further test the accuracy of this PES. In a first step, band assignments guided by the calculated VRT states, and rovibrational analyses of five  $v_2=1\leftarrow 0$  transitions observed in ortho-NH<sub>3</sub>-Ar and para-NH<sub>3</sub>-Ar enabled us to derive precise spectroscopic parameters. Four of these excited states were not previously observed. Band centers of both the lower and upper states of the inversion doublet are exploited to determine the tunneling splitting of the  $v_2$  umbrella state. In a second step, these new infrared data are compared to the VRT levels and transitions calculated on the *ab initio* 4D PES in order to evaluate the accuracy of the *ab initio* results in predicting band origins, rovibrational states, inversion tunneling splittings and a manifold of Coriolis couplings in both ground and  $v_2$  states.

## 1 Theory

### 1.1 Potential energy surface

In order to assign the experimental bands, we have performed bound state calculations for the ground vibrational state of NH<sub>3</sub>-Ar and for the first excited  $v_2 = 1$  state of the umbrella vibration. These calculations are based on the potential energy surface (PES) presented in Refs. [12, 16]. The PES depends on four coordinates: the distance  $R$  between the argon atom and the center of mass of the ammonia molecule, two angles  $\Theta$  and  $\varphi$  that define the orientation of NH<sub>3</sub> in the complex, and the coordinate  $\rho$  that describes the umbrella vibrational motion. In the ground state of free NH<sub>3</sub>, the equilibrium value is  $\rho = 112.15^\circ$ , while  $\rho = 90^\circ$  corresponds to planar NH<sub>3</sub>. The PES was constructed by computing the interaction energy at 6820 geometries by means of the coupled-cluster method with single, double, and perturbative triple excitations [CCSD(T)] with the AVQZ-DK basis set supplemented by midbond functions using the MOLPRO package. At the global minimum of the PES, the depth of the potential is 147.6 cm<sup>-1</sup>. The accuracy of the PES has been assessed in several ways. In its application to NH<sub>3</sub>-Ar scattering experiments, good agreement was found between calculated and measured differential and integral cross sections.<sup>17,18</sup> Applying it in bound state calculations on the NH<sub>3</sub>-Ar complex in the ground vibrational state of NH<sub>3</sub>, the computed rovibrational energy levels and rotational constants were found to be in excellent agreement with the available experimental spectra.<sup>12</sup>

### 1.2 Bound states

Our bound state calculations of NH<sub>3</sub>-Ar are based on the following Hamiltonian

$$H = H_{\text{int}} - \frac{\hbar^2}{2\mu R} \frac{\partial}{\partial R^2} R + \frac{1}{2\mu R^2} (J^2 + j^2 - 2\mathbf{j} \cdot \mathbf{J}) + V(R, \theta, \varphi, \rho) \quad (1)$$

where  $\mu$  is the reduced mass of the system,  $\mathbf{j}$  is the angular momentum operator describing the rotation of NH<sub>3</sub> in the complex, and  $\mathbf{J}$  is the total angular momentum operator. This is a special form of the Hamiltonian for molecule-molecule complexes

in body-fixed coordinates derived in Refs.[19,20]. The Hamiltonian  $H_{\text{int}}$  of the  $\text{NH}_3$  monomer is given by

$$H_{\text{int}} = \sum_i \frac{j_i^2}{2I_{ii}(\rho)} + T(\rho) + V_{\text{umb}}(\rho) \quad (2)$$

Where  $i = x, y, z$  and the  $I_{ii}$  are the corresponding principal moments of inertia. The operator  $T(\rho)$  is the kinetic operator for the curvilinear umbrella motion<sup>21</sup>, while  $V_{\text{umb}}(\rho)$  is an analytical function describing the double well potential of  $\text{NH}_3$  in the  $\rho$  coordinate<sup>22</sup>

$$V_{\text{umb}}(\rho) = \frac{k_\rho}{2} \left( \rho - \frac{\pi}{2} \right)^2 + a_\rho \exp \left[ -b_\rho \left( \rho - \frac{\pi}{2} \right)^2 \right] \quad (3)$$

The parameters in this function are  $k_\rho = 92026 \text{ cm}^{-1} \text{ rad}^{-2}$ ,  $a_\rho = 23383 \text{ cm}^{-1}$ , and  $b_\rho = 3.205 \text{ rad}^{-2}$ . With these parameters, the Hamiltonian of Eq. (2) with the potential of Eq. (3) accurately reproduces the experimental tunneling frequencies in the ground ( $v_2 = 0$ ) and first excited ( $v_2 = 1$ ) umbrella vibrational states (0.79  $\text{cm}^{-1}$  and 35.2  $\text{cm}^{-1}$ , respectively), as well as the  $v_2 = 0 \rightarrow 1$  excitation frequency of 949.9  $\text{cm}^{-1}$ .

The Hamiltonian is diagonal in the quantum numbers  $J$  (total angular momentum) and  $M$  (its projection on the space-fixed  $z$  axis). The states are also labeled by the quantum number  $K$ , the projection of  $J$  on the van der Waals bond axis  $\mathbf{R}$ , although this is not an exact quantum number due to the Coriolis couplings that mix states with  $\Delta K = \pm 1$ . States with  $K = 0$  are called  $\Sigma$  states, states with  $K = 1$  are called  $\Pi$  states.

The eigenstates of the Hamiltonian in Eq. (1) were obtained by a variational approach<sup>23,24,25,26,27</sup> with the basis of functions

$$|j, k, K, J, M, n, v\rangle = \left[ \frac{(2j+1)(2J+1)}{32\pi^3} \right]^{\frac{1}{2}} D_{Kk}^{(j)}(0, \theta, \varphi) * D_{MK}^{(J)}(\alpha, \beta, \gamma) * \frac{\chi_n(R)}{R} \Phi_v^\pm(\rho) \quad (4)$$

where  $j$  and  $k$  are the rotational quantum numbers of  $\text{NH}_3$ , and  $D$  denotes the Wigner functions. The angles  $(\alpha, \beta, \gamma)$  are the overall rotation angles of the complex:  $\beta$  and  $\alpha$  are the polar angles of the vector  $\mathbf{R}$  with respect to the space-fixed frame and  $\gamma$  describes the rotation of the complex about  $\mathbf{R}$ . The subscript  $v$  in  $\Phi_v^\pm(\rho)$  denotes the umbrella vibrational quantum number and the superscript  $\pm$  labels the symmetric and antisymmetric umbrella tunneling components of each  $v$ , while  $\chi_n(R)/R$  is a set of radial basis functions. Experimentalists often use the labels  $s$  and  $a$  to denote the

symmetric and antisymmetric inversion tunneling states of the complex, and we follow this convention elsewhere in this paper.

In a first step, the four functions  $\Phi_v^\pm(\rho)$  corresponding to  $v_2 = 0$  and  $v_2 = 1$ , were obtained by solving the one-dimensional Schrödinger equation with the Hamiltonian of Eq. (2) in a sinc function discrete variable representation.<sup>28,29</sup> The first two functions  $v = 0^\pm$  were employed in the basis (4) for the bound state calculations for  $v_2 = 0$ , while the next two functions  $v = 1^\pm$  were selected to construct the basis for  $v_2 = 1$ . The calculation of the bound states for  $v_2 = 0$  thus differs slightly from that of Ref. [12] in which all four  $\Phi_v^\pm(\rho)$  functions were included in the basis set; the resulting difference in the rovibrational energies is negligible.

In a second step, the functions  $\chi_n(R)$  were obtained using an effective radial potential of the form<sup>25</sup>  $V_{eff} = \alpha[V_0(R) - \zeta R]$ , where  $V_0(R)$  is a radial cut through the minimum of the 4D PES. The parameters  $\alpha$  and  $\zeta$  were optimized by minimizing the energy of the lowest rovibrational state of the NH<sub>3</sub>-Ar complex with five eigenfunctions  $\chi_n(R)$ . The optimized values are  $\alpha = 1$  and  $\zeta = 1 \times 10^{-3} E_h/a_0$ .

Finally, the rovibrational bound states of NH<sub>3</sub>-Ar were calculated with a basis with  $j_{max} = 10$  and 20 functions  $\chi_n(R)$  calculated on an equidistant grid of 110 points from 4.5 to 20  $a_0$ . For each irreducible representation (irrep) of the full molecular symmetry group  $D_{3h}(M)$ , we calculated the lowest 20 eigenvalues of the Hamiltonian for each  $J$  ranging from 0 to 10 by means of the iterative algorithm of Davidson.<sup>30</sup> The irreps are  $A'_1, A''_1, A'_2, A''_2, E', E''$ . Eigenstates carrying irreps  $A'_2, A''_2$  belong to ortho-NH<sub>3</sub>-Ar, with nuclear spin statistical weight 12, states carrying irreps  $E', E''$  belong to para-NH<sub>3</sub>-Ar, with nuclear spin weight 6, while states carrying irreps  $A'_1, A''_1$  are Pauli-forbidden. In the calculations of the one-dimensional irreps  $A'_1, A''_1, A'_2, A''_2$  the basis in Eq. (4) could be restricted to functions with the NH<sub>3</sub> quantum number  $k = 0$  (modulo 3). For the  $E', E''$  irreps only basis functions with  $k = 1$  (modulo 3) are needed; the basis functions with  $k = -1$  (modulo 3) correspond to the other component of these two-dimensional irreps and yield the same energy levels. The  $A'_1, A'_2, E'$  states have + parity under inversion, the  $A''_1, A''_2, E''$  states have - parity.

### 1.3 Intensities

In order to obtain a complete *ab initio* prediction of the spectra, we use the wave functions from the bound state calculations to compute line strengths of all allowed  $\Delta J = 0, \pm 1$  transitions between the VRT states of the NH<sub>3</sub>-Ar complex for total  $J = 0 - 10$  that accompany the  $v_2 = 0 \rightarrow 1$  transition of the NH<sub>3</sub> monomer. The formulas used to compute the line strengths are taken from Ref. [31], where they have been explicitly derived. *Ab initio* absorption spectra are then computed from the line strengths by assuming a Boltzmann distribution (at some rotational temperature) of the lower states, and summing over all allowed transitions to the upper states.

The  $v_2 = 0 \rightarrow 1$  transition is a parallel vibration-tunneling transition of  $\text{NH}_3$ , which obeys the selection rules  $A'_2 \leftrightarrow A''_2$  and  $E' \leftrightarrow E''$ . That is, it is allowed between the symmetric (lower) umbrella-inversion tunneling state of the vibrational ground state and the antisymmetric (upper) inversion state of the  $v_2 = 1$  state, and vice versa. Since the tunneling splitting is  $0.79 \text{ cm}^{-1}$  in the  $v_2 = 0$  state and as large as  $35.2 \text{ cm}^{-1}$  in the  $v_2 = 1$  state this gives rise to two series of lines centered around  $968$  and  $932 \text{ cm}^{-1}$ , respectively. However, the ortho- $\text{NH}_3$ -Ar complex is bound by  $94 \text{ cm}^{-1}$  and the para- $\text{NH}_3$ -Ar complex by  $98 \text{ cm}^{-1}$  and the inversion-tunneling splittings are in some cases altered with respect to free  $\text{NH}_3$ .<sup>12</sup> Moreover, the states of even parity of the complex,  $A'_2$  and  $E'$ , contain both the even and odd parity states of the  $\text{NH}_3$  monomer, and so do the states of odd parity,  $A''_2$  and  $E''$ . Hence, the rovibrational transitions of the complex that accompany the vibration-tunneling transitions on the  $\text{NH}_3$  monomer cover a large range of frequencies. Since we are only interested in the relative line strengths, the two (nearly equal) transition dipole moments of the parallel vibration-tunneling transitions in  $\text{NH}_3$  were set equal to 1. Absolute line strengths can be obtained by multiplication with the square of the actual transition dipole moment.

## 2- Experimental

The rovibrational spectra in the region of the  $v_2$  umbrella mode of  $\text{NH}_3$ -Ar were recorded using a jet-cooled laser spectrometer recently developed at the MONARIS laboratory. This set-up couples an external-cavity quantum cascade laser (EC-QCL) with a pulsed supersonic jet to realize direct absorption in the jet and has already been described in detail in recent papers.<sup>32,33</sup> Only the main characteristics will be presented hereafter.

As clearly demonstrated in many previous jet-cooled studies, the combined use of very diluted molecular samples seeded in high backing pressures of carrier gas enabled to obtain an efficient rovibrational cooling and to stabilize weakly bound complexes.  $\text{NH}_3$ -Ar complexes are produced in a planar supersonic expansion using ternary He/Ar/ $\text{NH}_3$  mixtures with typically 2%  $\text{NH}_3$  and Ar/He = 2/1 and optimal backing pressures of 3 bar. The light source is a continuous-wave room-temperature mode hop-free EC-QCL with a spectral width of 10 MHz, which covers the  $930\text{--}990 \text{ cm}^{-1}$  range (Daylight Solutions). About 8% of the total light is sent through two additional laser channels for relative and absolute frequency calibrations. Relative frequencies are monitored by measuring the intensity transmitted through a solid germanium etalon with a free spectral range of 490 MHz, to provide a relative frequency scale. Absolute laser frequencies are obtained by measuring the transmission through a 15 cm-length reference cell containing a known reference gas at a pressure of about 5 mbar (ethene in the present work). The main part of the light is sent through a multipass optical cavity mounted in the jet chamber, which is evacuated by a  $2000 \text{ l s}^{-1}$  oil diffusion pump backed by a combination of a  $350 \text{ m}^3 \text{ h}^{-1}$  Roots blower and a  $40 \text{ m}^3 \text{ h}^{-1}$  rotary pump. The optical configuration used for the present study is an astigmatic cavity composed of two 1.5" astigmatic mirrors ( $R = 99.2\%$ , AMAC-36, Aerodyne Research) aligned according to a 182-pass

configuration. Three liquid-nitrogen cooled HgCdTe detectors (Judson J15D12) are used to measure the powers transmitted through the multipass cavity, the etalon and the reference gas cell. The molecular jet is produced by a pulsed nozzle (General Valve Series 9) by fitting a 0.9 mm diameter pin hole nozzle with two modified industrial blades, forming a 30 mm length x 50  $\mu\text{m}$  width slit opening, and serving as the molecular expansion source. Rovibrationally cooled complexes were probed by the infrared laser light at short distances, not larger than 3 mm from the nozzle exit to keep a sufficient density of van der Waals complexes to be probed in the slit jet expansion. Our rapid scan scheme described in detail elsewhere is close to the original designs used for high resolution molecular spectroscopy.<sup>34</sup> Fine tuning of the laser frequency over about 0.8  $\text{cm}^{-1}$  at a repetition rate of 100 Hz is obtained by a sine wave generated by a Labview code and delivered to a piezoelectric transducer attached to the diffraction grating that ends the external cavity. The intensities transmitted through the supersonic jet, the etalon and the reference gas cell are digitized and recorded simultaneously as a function of time. A baseline-free transmittance through the multipass cavity is then obtained by taking the ratio of the corresponding signals recorded with and without the jet. The procedure for absolute frequency calibration is achieved in real time by measuring the deviation between experimental and HITRAN12<sup>35</sup> database  $\text{C}_2\text{H}_4$  frequencies after each laser sweep to correct the free spectral range value of the etalon fixed at the beginning of each experiment. The accuracy of the frequency calibration is around 0.0005  $\text{cm}^{-1}$ . While the line width of the QCL source is typically 20 MHz, the resolution (full-width-at-half-maximum, FWHM) of isolated rovibrational lines achieved with the jet-cooled QCL spectrum is about 75(10) MHz, limited by both residual Doppler broadening at the temperature of the expansion and a small contribution (dependent on mass of carrier gas) from non orthogonal laser and planar jet crossings in the multi pass optical cavity.

### 3- Results

#### 3-1 Energy level scheme of the $\nu_2$ transition of $\text{NH}_3\text{-Ar}$

Our high resolution infrared jet-cooled measurements in the  $\nu_2$  umbrella region of  $\text{NH}_3\text{-Ar}$  are guided by many theoretical and experimental studies realized over thirty years. The pioneering microwave study of Fraser et al.<sup>3</sup> evidenced a series of ground state transitions interpreted with a model of the  $\text{NH}_3$  molecule almost freely rotating due to a nearly isotropic interaction potential. In the  $\nu_2$  region the observation of several laser coincidences with rovibrational lines of  $\text{NH}_3\text{-Ar}$  was interpreted as a proof that the  $\text{NH}_3$  inversion frequency is practically unchanged upon complexation.<sup>13,14</sup> Here, we further investigate this assumption and provide a precise determination of the inversion splitting in the  $\nu_2$  state.

Figure 1 displays the internal rotor energy levels of  $\text{NH}_3\text{-Ar}$  for the  $\nu_2=1\leftarrow 0$  transition with their two distinct nuclear-spin modifications noted ortho and para.

Only the ground vibrational state energy levels thermally populated in a pulsed supersonic expansion are shown in the scheme, i.e., the lowest ortho state labeled by  $\Sigma_a(j,k=0)$  and three para states labeled by  $\Sigma_s(j,k=1)$ ,  $\Sigma_a(j,k=1)$  and  $\Pi_s(j,k=1)$ , located 12.45, 13.2069 and 13.9603  $\text{cm}^{-1}$  above  $\Sigma_a(j,k=0)$ , respectively. The notations  $\Sigma$  ( $K=0$ ) and  $\Pi$  ( $K=1$ ) indicate the projection  $K$  of the total rotational angular momentum  $J$  on the vdW bond axis, the subscripts  $s$  and  $a$  designate a symmetric or antisymmetric  $\text{NH}_3$  inversion wave function, and the state labels  $j$  and  $k$  are only approximate quantum numbers in the complex that indicate the correlation between the internal rotor state of the complex and the  $j$ ,  $k$  rotational state of the free  $\text{NH}_3$  monomer.

Accurate energy values for the ground states of ortho and para  $\text{NH}_3\text{-Ar}$  were obtained from microwave and submillimeter-wave measurements.<sup>5,6,7,8,9</sup> Five  $v_2=1\leftarrow 0$  transitions of  $\text{NH}_3\text{-Ar}$  were observed with our jet-cooled infrared laser spectrometer: the two ortho transitions are easily assignable due to the presence of a single initial state and the absence of Coriolis couplings in both ground and excited states. They correspond to  $\Pi_s(j=1,k=0)\leftarrow \Sigma_a(j,k=0)$  and  $\Sigma_s(j=1,k=0)\leftarrow \Sigma_a(j,k=0)$  transitions with the final states shown in Figure 1. Table 1 lists the observed transitions for the two bands of ortho- $\text{NH}_3\text{-Ar}$ . Three additional transitions were also observed in the 938, 970 and 974  $\text{cm}^{-1}$  regions, More challenging assignments to the  $\Pi_{s/a,\text{lower}}(j,k=1)\leftarrow \Sigma_a(j,k=1)$  and both  $\Pi_{s/a,\text{upper}}(j,k=1)\leftarrow \Sigma_s(j,k=1)$  transitions in para- $\text{NH}_3\text{-Ar}$  will be justified in detail hereafter. Table 2 lists the observed transitions for the three bands of para- $\text{NH}_3\text{-Ar}$ . The energies of ortho transitions observed correspond to band centers derived from the rovibrational analysis while those of the para transitions correspond to Q(0) line frequencies extrapolated from the Q branch (very close to the band centers). The relative energies of the para and ortho  $\text{NH}_3\text{-Ar}$  stacks shown in Figure 1 are extracted from the ground state VRT levels presented by Loreau et al.<sup>12</sup>

### 3-2 Jet-cooled laser spectra results

In the following, we present the five rovibrational bands observed in the region of the  $v_2=1\leftarrow 0$   $\text{NH}_3$  monomer band. The two most intense bands characterized by the absence of rotational perturbation are ascribed to  $\text{NH}_3\text{-Ar}$  ortho complexes. The three weaker ones are strongly perturbed and unambiguous transition assignments require the use of our *ab initio* calculated VRT levels and  $v_2 = 0 \rightarrow 1$  transition frequencies and intensities.

#### 3-2-1 Ortho $\text{NH}_3\text{-Ar}$ complexes

Figure 2a displays the jet-cooled spectrum of the  $\Pi_s(j=1,k=0)\leftarrow \Sigma_a(j,k=0)$  transition. This spectrum resembles that of a  $\Pi \leftarrow \Sigma$  type vibrational band of a linear molecule, confirmed by the presence of an R(0) transition and a strong Q branch and the absence of a P(1) transition. As seen in Fig. 2a, the Q branch degrades to the low frequency side but we were unable to resolve the individual Q branch lines. This band was already observed by Fraser et al.<sup>13</sup>, but only partially due to the lack of side-band coverage of the lamb-dip stabilized  $\text{CO}_2$  laser in this region. Thanks to its much higher resolution attainable ( $\sim 1$  MHz)

Fraser et al. could determine the  $l$ -type doubling constant  $q$  which is involved in the expression of the energy of  $P$ ,  $Q$  and  $R$  transitions for the ground and excited states:

$$E(\pm, J, l) = \nu_0 + B[J(J + 1) - l^2] \pm (q/2)J(J + 1) \pm q_J J(J + 1)^2 \quad (5)$$

where for the ground state,  $\nu_0$ ,  $l$ ,  $q$  and  $q_J = 0$ .  $q$  is the  $l$ -type doubling constant, the + sign is taken for the upper state in the  $Q$ -branch transition and the - sign is taken for the upper state in the  $P$ - and  $R$ -branch transitions of the  $l$ -doubled pair in the excited state.

The positive value of  $q$  (90.928 MHz) derived from the least squares fit of Fraser et al.<sup>13</sup> provided information about the location of neighboring  $\Sigma$ -type states that are Coriolis coupled to the observed  $\Pi$  state and confirmed that the dominant  $\Sigma$  perturbing state is above the  $\Pi$  state, by about  $12 \text{ cm}^{-1}$  using a pure precession model.<sup>13</sup> Figure 2b displays our global fit of the  $\Pi_s(j=1, k=0)$  state parameters using the PGOPHER software<sup>36</sup> with 25 rotational lines, 18  $R(J)$  and  $P(J)$  lines from the present study and 7  $Q(J)$  lines determined at sub MHz precision by Fraser et al.<sup>13</sup>

Figure 3a displays the jet-cooled spectrum of the  $\Sigma_s(j=1, k=0) \leftarrow \Sigma_a(j, k=0)$  transition never observed previously. The absence of a  $Q$  branch confirms the assignment of a  $\Sigma \leftarrow \Sigma$  type vibrational band. The spectrum is slightly blurred by intense  $\text{NH}_3$  monomer lines but the simulation (Fig. 3b) well matches the observed one with a rms error of about 5 MHz for 23 rovibrational lines and a rotational temperature of about 3 K. Table 3 lists the molecular parameters derived from the simulation of both rovibrational band contours, as well as the values extracted from a fit to the VRT levels that we calculated for total angular momentum  $J$  values up to 10.

### 3-2-2 Para $\text{NH}_3$ -Ar complexes

Figure 4a displays the jet-cooled spectrum observed in the  $936.8\text{-}939.4 \text{ cm}^{-1}$  region where we expected to observe the lower component of the inversion doublet. The spectrum is quite puzzling due to the presence of several overlapping series of rotational lines with strongly unequal spacings, characteristic of Coriolis couplings. Another difficulty is related to the weakness of the observed para transitions. There are three reasons why these transitions are weaker than the ortho transitions: i) the relative population of ortho and para states is determined by the nuclear spin weights, which are 12 and 6, respectively, ii) the population of the para states is shared by three low-lying states and iii) the line strengths of the para lines are generally smaller in  $\text{NH}_3$ -Ar.

Taking advantage of microwave transitions assigned for the  $\text{NH}_3$ -Ar states correlating with  $\text{Ar} + \text{NH}_3$  ( $j=1, |k|=1$ ) by Zwart et al.<sup>8</sup>, we are able to provide combination differences in the ground state allowing us to check the initial state of the observed transitions. We found a remarkable agreement between the energy difference measured by submillimeter spectroscopy between the  $J=2$  and  $J=4$  levels

of the  $\Sigma_a(j=1, k=1)$  state and that between two rotational lines observed at 938.4191 and 937.2592  $\text{cm}^{-1}$ , both equal to 1.1598  $\text{cm}^{-1}$ . This allowed us to assign these lines to R(2) and P(4), respectively. Moreover, our attributions are confirmed by the microwave-infrared double resonance measurements of Fraser<sup>13</sup> who tentatively assigned two CO<sub>2</sub> laser coincidences at 937.1656 and 938.6893  $\text{cm}^{-1}$  to P(5) and R(3) lines of the  $\Pi_{s/a, \text{lower}}(j=1, k=1) \leftarrow \Sigma_a(j=1, k=1)$  transition, very close to the lines observed in the present study at 937.1658 and 938.6896  $\text{cm}^{-1}$ . Finally our calculated VRT levels, transition frequencies, and line strengths are used to provide a definite proof of this assignment: on the basis of energy and relative line strengths only one  $v_2=1 \leftarrow 0$  transition of NH<sub>3</sub>-Ar is compatible with our observations in the investigated region, namely the  $\Pi_{s/a, \text{lower}}(j=1, k=1) \leftarrow \Sigma_a(j=1, k=1)$  transition. According to the selection rules of *l*-doubling in a  $\Pi \leftarrow \Sigma$  transition, P and R branch lines terminate on rotational levels of the same parity ( $a \leftrightarrow a$ ) as opposed to the Q branch lines that terminate on rotational levels of the opposite parity ( $a \leftrightarrow s$ ).<sup>37</sup> Figure 4b displays the theoretical spectrum of the  $\Pi_{s/a, \text{lower}}(j=1, k=1) \leftarrow \Sigma_a(j=1, k=1)$  transition weighted by a rotational population at 3 K. Q branch lines were slightly shifted in frequency, as well as P and R branch lines to obtain a correct absolute frequency agreement with the jet-cooled spectrum.

In the same manner, Figure 5a displays the jet-cooled spectrum observed in the 973.2-976.6  $\text{cm}^{-1}$  region where we expected to observe the upper component of the inversion doublet. Spectral assignments are not straightforward either except for the Q branch pattern clearly observed around 974.5  $\text{cm}^{-1}$ . Following the same approach as for the lower component region, an excellent match is found between the energy difference of 1.1988  $\text{cm}^{-1}$  separating the  $J=2$  and  $J=4$  levels of the  $\Sigma_s(j=1, k=1)$  state and that between two rotational lines observed at 975.0561 and 973.8573  $\text{cm}^{-1}$ , which enabled us to assign these lines to R(2) and P(4), respectively. Again our *ab initio* calculated results nicely confirm this preliminary assignment as proved by the very good agreement between the jet-cooled and the theoretical spectrum of the  $\Pi_{s/a, \text{upper}}(j=1, k=1) \leftarrow \Sigma_s(j=1, k=1)$  transition (Fig. 5b) shifted in frequency by the same value for all branches.

Lastly, Figure 6 displays the jet-cooled spectrum observed in the 969.3-972.5  $\text{cm}^{-1}$  region. Our calculation of the VRT levels of the  $v_2$  state predicts a second  $\Pi_{s/a, \text{upper}}(j=1, k=1)$  state of the same symmetry and with the same approximate quantum numbers as the first  $\Pi_{s/a, \text{upper}}(j=1, k=1)$  state, but lower in energy by -3.536  $\text{cm}^{-1}$  (see Figure 1). A second  $\Pi_{s/a, \text{upper}}(j=1, k=1) \leftarrow \Sigma_s(j=1, k=1)$  transition is indeed observed in this region, but it is less intense, in agreement with the smaller line strengths calculated. Only the Q and R branches are clearly observed and assigned [as for example the Q(2) line corresponding to the CO<sub>2</sub> laser coincidence observed by Bizzari et al.<sup>14</sup> at 970.5498  $\text{cm}^{-1}$ ], while the P branch displays a confused pattern of weak lines that makes a reliable assignment difficult. Actually, the calculated VRT levels predict two transitions likely to be observed in this region, terminating in the nearby states  $\Pi_{s/a, \text{upper}}(j=1, k=1)$  and  $\Delta_{s/a}(j=2, k=2)$  with an intensity ratio of 4/1. The calculated Q branch pattern of the  $\Delta_{s/a}(j=2, k=2) \leftarrow \Sigma_s(j=1, k=1)$  transition nicely

reproduces the asymmetry on the high frequency side observed in the jet-cooled spectrum, while the  $\Pi_{s/a,upper}(j=1,k=1) \leftarrow \Sigma_s(j=1,k=1)$  transition does not. It fails to reproduce the rovibrational spacings, however, so we essentially assign the band in this region to the  $\Pi_{s/a,upper}(j=1,k=1) \leftarrow \Sigma_s(j=1,k=1)$  transition. As discussed in Section 4, the nearby states  $\Pi_{s/a,upper}(j=1,k=1)$  and  $\Delta_{s/a}(j=2,k=2)$  are very strongly mixed by Coriolis coupling.

From the assignment of the observed para-NH<sub>3</sub>-Ar transitions, we could determine two different inversion splittings in the  $v_2$  state. Due to probable Coriolis couplings within these transitions it is not possible to correctly reproduce the observed spectra to extract precise band centers. According to the diagram energy level in Figure 1, the splittings between the  $\Pi_{s/a,lower}(j=1,k=1) \leftarrow \Sigma_a(j=1,k=1)$  transition and each of the two  $\Pi_{s/a,upper}(j=1,k=1) \leftarrow \Sigma_s(j=1,k=1)$  transitions in para-NH<sub>3</sub>-Ar observed and analyzed in the present study correspond to the sum of the  $\Sigma_a$ - $\Sigma_s$  splitting of 22.691 GHz determined precisely in the ground state and two different inversion splittings in the  $v_2$  state. Using extrapolated Q(0) frequency values of 937.6621 cm<sup>-1</sup> for the lower band, and 970.4215 and 974.4268 cm<sup>-1</sup> for the two higher bands, we derived inversion splittings of 32.003(1) and 36.008(1) cm<sup>-1</sup>. These values are of roughly the same size as the corresponding inversion splitting in free NH<sub>3</sub>.

These findings imply that the inversion splitting pattern in the  $v_2=1$  excited state is qualitatively different from that in the ground state. Loreau et al.<sup>12</sup> found for the ground state that the inversion splitting of the  $\Sigma$  levels is nearly unchanged with respect to free NH<sub>3</sub>, while in the  $\Pi$  states inversion tunneling is nearly quenched and the level splitting is very small. All  $v_2=1$  excited states involved in the transitions observed here are  $\Pi$  states, but we still find inversion splittings nearly as large as in free NH<sub>3</sub>. A detailed picture of the inversion tunneling in both the  $v_2=0$  and  $v_2=1$  states can be obtained by careful inspection of our *ab initio* calculated VRT levels and wave functions. Also the Coriolis couplings that are important in the observed para NH<sub>3</sub>-Ar spectra can be understood from the analysis of the wave functions, because we explicitly take this type of perturbation into account in our calculations. These points will be examined below.

#### 4- Discussion

New reliable infrared data are derived from the band contour analysis of rovibrational jet-cooled spectra of two ortho and three para  $v_2=1 \leftarrow 0$  transitions. For the  $\Pi_s(j=1,k=0) \leftarrow \Sigma_a(j,k=0)$  band, the molecular parameters for the  $\Pi_s(j=1,k=0)$  state determined by Fraser<sup>13</sup> using Lamb dip spectroscopy are more accurate than ours by about a factor 20. We note, however, a difference of about 0.004 cm<sup>-1</sup> between the respective band origins. Our accuracy in the absolute frequency from calibration based on the correction of the free spectral range of the etalon after measuring the deviation between about fifty experimental and HITRAN<sup>35</sup> C<sub>2</sub>H<sub>4</sub> frequencies over the 949-951.5 cm<sup>-1</sup> range, is about 10 times less than the difference reported between

both measurements. Therefore, we are confident that the band origin value determined in the present study is correct.

More generally, we could determine with a very good precision the band origins of five  $\nu_2$  states. The energy difference between the ortho states  $\Sigma_s(j=1, k=0)$  and  $\Pi_s(j=1, k=0)$ , equal to  $10.34974 \text{ cm}^{-1}$ , is now corrected with respect to the estimated value ( $12.1 \text{ cm}^{-1}$ ) of Fraser<sup>13</sup> and can be used to refine predictive models. Even though we could not determine the band origin of the para bands with the same precision as for the ortho ones, the extrapolated Q(0) line frequencies reported in Figure 1 are sufficiently reliable to determine whether our new infrared data related to the  $\nu_2$  mode of NH<sub>3</sub>-Ar agree with our *ab initio* calculated frequencies. From the energies and wave functions of the VRT states of the complex we computed transition frequencies and line strengths, from which we generated theoretical spectra at the experimental rotational temperature for the five bands observed. For the ortho bands, the experimental band origins are reproduced to within  $0.04$  and  $0.74 \text{ cm}^{-1}$  for the  $\Pi_s(j=1, k=0)$  and  $\Sigma_s(j=1, k=0)$  states, respectively, and the rotational constants  $B$  differ by at most  $0.4\%$  from the experimental values. For the para bands, the maximum deviation is  $0.38 \text{ cm}^{-1}$  for the band origins. Table 4 displays a comparison between band centers (or Q(0) line positions) of the five  $\nu_2=1 \leftarrow 0$  transitions of NH<sub>3</sub>-Ar observed and calculated *ab initio*. Our experimentally determined tunneling splittings of the  $\nu_2$  state of  $32.003$  and  $36.008 \text{ cm}^{-1}$  agree well with the values of  $32.09$  and  $35.51 \text{ cm}^{-1}$  predicted by the extrapolated Q(0) lines from the *ab initio* calculated VRT levels.

The inversion tunneling pattern in the  $\nu_2=1$  excited states, which is qualitatively different from that in the ground state,<sup>12</sup> can be understood by analysis of the *ab initio* calculated wave functions. In the lower component of the inversion doublet in para NH<sub>3</sub>-Ar excited in the band at  $937.6621 \text{ cm}^{-1}$  the umbrella wave function of the NH<sub>3</sub> monomer in the complex is a pure symmetric inversion state. This implies that inversion is nearly unhindered, as in free NH<sub>3</sub>, even though this state is a  $\Pi$  state. The upper component of the inversion doublet is actually split into two  $\Pi$  levels. In the lower one of these levels, accessed by the band at  $970.4220 \text{ cm}^{-1}$ , the NH<sub>3</sub> umbrella wave function contains  $65\%$  of the symmetric inversion state and  $35\%$  of the antisymmetric one. In the higher one, accessed by the band at  $974.4268 \text{ cm}^{-1}$ , the umbrella wave function has  $43\%$  of symmetric and  $57\%$  of antisymmetric inversion character. This implies that the NH<sub>3</sub> inversion tunneling is hindered by the interaction with Ar and that the umbrella wave functions are more or less localized in one or the other of the wells of the double-well inversion potential. In such a complicated case, the question is how to define the inversion splittings. Adopting the conventional picture from the literature, we chose to identify the two inversion splittings of  $32.003$  and  $36.008 \text{ cm}^{-1}$  with the frequency differences between the origins of the bands at  $970.4215$  and  $974.4268 \text{ cm}^{-1}$  and the band at  $937.6621 \text{ cm}^{-1}$ . However, since the character of the upper states accessed by the bands at  $970.4220$  and  $974.4268 \text{ cm}^{-1}$  indicates that inversion tunneling is nearly quenched in these states, it would perhaps be better to consider the frequency difference of  $4.005 \text{ cm}^{-1}$  between the origins of these upper states as the inversion splitting.

The very good reproduction of rovibrational band patterns of three para bands terminating on the lower and upper components of the inversion doublet (Figures 4, 5 and 6) nicely proves that the Coriolis couplings included in our calculations of the VRT levels give a realistic picture of the internal dynamics in the  $\nu_2$  mode. More information can be now be extracted about the relative contribution of these couplings for the five  $\nu_2$  para states involved in this study, namely  $\Sigma_a(j=1,k=1)$ ,  $\Sigma_s(j=1,k=1)$ ,  $\Pi_{s/a,lower}(j=1,k=1)$  and  $\Pi_{s/a,upper}(j=1,k=1)$ , where the latter state has two components separated by about  $4\text{ cm}^{-1}$ .

We illustrate the importance of Coriolis coupling in the excited para states  $\Pi_{s/a,upper}$  and  $\Pi_{s/a,lower}$  with nearby states by comparing the relative weights of the final states. For the  $\Pi_{s/a,lower}(j=1,k=1)$  state, the relative weight of the  $\Pi$  state is higher than 99.3% for all  $J$ . This state is weakly coupled with the  $\Sigma_{a,s}(j=1,k=1)$  state,  $4.95\text{ cm}^{-1}$  lower in energy. For the highest  $\Pi_{s/a,upper}(j=1,k=1)$  state, the relative weight of the  $\Pi$  component decreases from 99.9 to 89.5% as  $J$  increases from 1 to 8. It is therefore more strongly coupled than the lower  $\Pi$  state, with three closer states, namely  $\Sigma_a(j=1,k=1)$  (not shown in Fig. 1) and  $\Delta_{s/a}(j=2,k=2)$ , which are  $4.05$  and  $3.194\text{ cm}^{-1}$  lower in energy, respectively and  $\Delta_{s/a}(j=2,k=1)$ , which is  $2.247\text{ cm}^{-1}$  higher (Figure 1). The contribution of  $\Sigma$  and  $\Delta$  states coupled to  $\Pi_{s/a,upper}(j=1,k=1)$  is almost equal. It is not surprising that Coriolis coupling is stronger in this  $\Pi_{s/a,upper}(j=1,k=1)$  state, due to the presence of three states closer in energy. The lowest  $\Pi_{s/a,upper}(j=1,k=1)$  state lies even closer to the  $\Delta_{s/a}(j=2,k=2)$  state, which implies that Coriolis coupling is still stronger. The weight of the  $\Pi$  component decreases from 99.7 to 63.4% when  $J$  increases from 1 to 8 and the nearby  $\Delta_{s/a}(j=2,k=2) \leftarrow \Sigma_s(j=1,k=1)$  transition clearly affects the band contour of the lowest  $\Pi_{s/a,upper}(j=1,k=1) \leftarrow \Sigma_s(j=1,k=1)$  transition. Accordingly, the  $\Delta_{s/a}(j=2,k=2)$  state contains a substantial amount of  $\Pi_{s/a,upper}(j=1,k=1)$  character, up to 35% for  $J = 8$ . Such a mixing of states is confirmed by the good match of the  $Q(J) \Delta \leftarrow \Sigma$  band contour with our observations.

Coriolis coupling is expected to be very strong also in the ground states of para  $\text{NH}_3\text{-Ar}$ , since the coupled state  $\Pi_{s/a}(j=1,k=1)$  is close in energy to the perturbing states: it is only  $1.51$  and  $0.76\text{ cm}^{-1}$  higher than  $\Sigma_s(j=1,k=1)$  and  $\Sigma_a(j=1,k=1)$ , respectively. Figure 7 displays the evolution of the relative weight of  $\Pi_{s/a}(j=1,k=1)$  of the lower states  $\Sigma_s(j=1,k=1)$  and  $\Sigma_a(j=1,k=1)$  as a function of the rotational quantum number  $J$ , extracted from our calculations of the VRT wave functions. A nearly linear increase of the coupling from 0 ( $J = 0$ ) to 15.11% ( $J = 8$ ) for  $\Sigma_s(j=1,k=1)$ , and from 0 to 19.71% for  $\Sigma_a(j=1,k=1)$  is observed, directly correlated with a decrease of the relative weight of  $\Pi_{s/a,upper}(j=1,k=1)$ . Hence, the accurate reproduction of the band contour pattern of most of observed transitions by our *ab initio* calculations allows us to claim that the unequal rovibrational spacings observed are mainly due to strong Coriolis coupling in the ground states for the  $\Pi_{s/a,lower}(j=1,k=1) \leftarrow \Sigma_a(j=1,k=1)$  transition, and in both ground and excited states for the  $\Pi_{s/a,upper}(j=1,k=1) \leftarrow \Sigma_s(j=1,k=1)$  transition.

Finally, Coriolis coupling contributes to the complexity of the assignment of rovibrational lines in both regions  $969.5\text{-}972.5\text{ cm}^{-1}$  and  $973.2\text{-}976.6\text{ cm}^{-1}$  since the

transitions  $\Delta_{s/a}(j=2,k=2)\leftarrow\Sigma_s(j=1,k=1)$  and  $\Delta_{s/a}(j=2,k=1)\leftarrow\Sigma_s(j=1,k=1)$ , are allowed by mixing of the  $\Delta_{s/a}(j=2,k=2)$  and  $\Delta_{s/a}(j=2,k=1)$  states with the two  $\Pi_{s/a,\text{upper}}(j=1,k=1)$  states. Our *ab initio* calculations predict that the Q branch of the weak  $\Delta_{s/a}(j=2,k=1)\leftarrow\Sigma_s(j=1,k=1)$  transition is expected to lie at about 975  $\text{cm}^{-1}$ .

## Conclusion

The tunable infrared laser spectrometer recently developed at MONARIS has been exploited to probe the rarely investigated  $\nu_2$  umbrella mode region of the  $\text{NH}_3\text{-Ar}$  van der Waals complex in a pulsed supersonic jet expansion. Our rovibrational study was guided by sub-MHz microwave-infrared double resonance experiments<sup>13</sup> and by calculations of the VRT levels based on a 4D potential energy surface from *ab initio* calculations that includes explicitly the umbrella inversion motion<sup>12</sup>.

Two bands in ortho- $\text{NH}_3\text{-Ar}$  and three bands in para- $\text{NH}_3\text{-Ar}$  were unambiguously assigned in the 936-975  $\text{cm}^{-1}$  region on the basis of a rovibrational analysis for the ortho ones, and by comparison with our *ab initio* calculated VRT levels and transitions for the para bands. The *ab initio* results for both the ortho and para species turn out to be very predictive in terms of band centers, upper state rotational constants, and relative weight of Coriolis couplings in the ground and excited  $\nu_2$  states. Moreover, the values of the tunneling frequencies derived from the calculated VRT states agree with the experimental values measured in the  $\nu_2$  state within an error not larger than 1.4 %.

As already highlighted in recent studies combining spectroscopy with high level *ab initio* calculations<sup>38,39</sup>, the present study demonstrates once again the interest to compare spectroscopic measurements and theoretical predictions based on *ab initio* calculated PESs in order to improve the understanding of weak interactions: the computation of multi-dimensional PESs and VRT spectra based on these potentials helps to unravel the rovibrational spectra of VdW complexes showing a rich internal dynamics, while a wealth of reliable spectroscopic data is needed to check and possibly improve the accuracy of a PES and to make it fully predictive. In the near future, other  $\text{NH}_3$ -containing complexes could be investigated in the  $\nu_2$  umbrella mode region with the same set-up to probe the asymmetry of the intermolecular PES with respect to the umbrella inversion motion.

## Acknowledgments

This work was supported by the MICHEM Labex at Sorbonne Université. AP acknowledges COST Action CM1401 “Our Astro-Chemical History”.

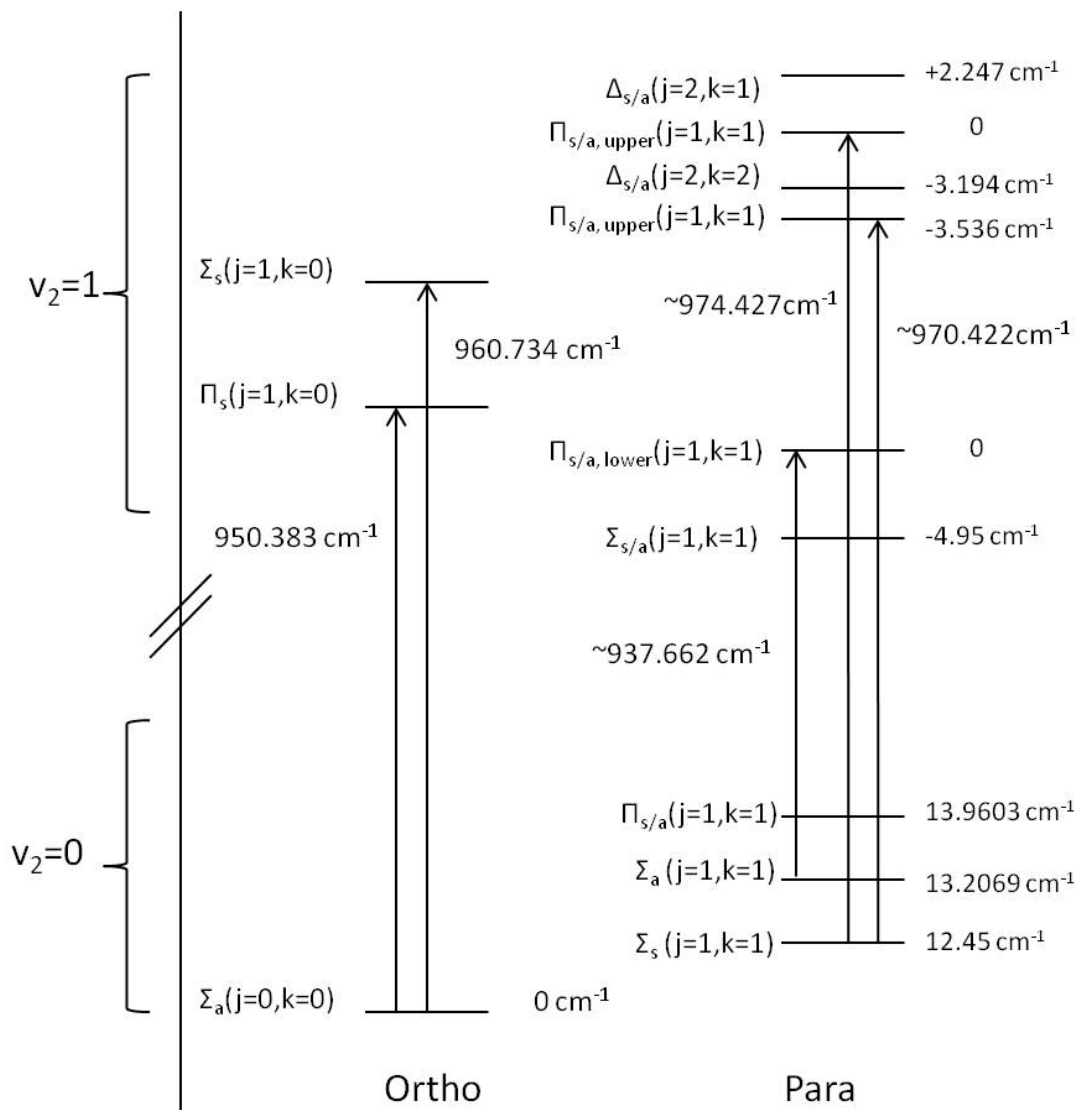


Figure 1: Lowest internal rotor energy levels in both  $v_2=0$  and  $v_2=1$  states of the  $v_2$  umbrella mode of  $\text{NH}_3\text{-Ar}$ . The five mid-infrared transitions observed are represented by bold type arrows. The energies reported for ortho transitions correspond to band centers derived from the fitting of rovibrational band contours. The energies reported for para transitions correspond to frequencies of Q(0) lines extrapolated from the rovibrationally resolved distribution of the Q branch. The  $\text{NH}_3\text{-Ar}$  states involved in this study are labeled by  $\Sigma(j, k)$ ,  $\Pi(j, k)$ ,  $\Delta(j, k)$  where  $\Sigma$ ,  $\Pi$ ,  $\Delta$  ... denote the projection of the total rotational angular momentum  $J$  on the vdW bond axis, while  $j$  and  $k$  give the correlation between the internal-rotor state of the complex and the  $j, k$  rotational states of the free  $\text{NH}_3$  monomer. Other  $\text{NH}_3\text{-Ar}$  states which are Coriolis coupled to the initial and final states of the observed transitions are written in italics. The energy difference of  $12.45 \text{ cm}^{-1}$  between the lowest ortho and para states corresponds to the difference between the calculated zero-point levels of ortho  $\text{NH}_3\text{-Ar}$  ( $-94.22 \text{ cm}^{-1}$ ) and para  $\text{NH}_3\text{-Ar}$  ( $-81.77 \text{ cm}^{-1}$ ).<sup>12</sup> Ground state para energies are given by Zwart et al.<sup>8</sup> The relative energies of the para  $v_2$  levels are derived from our *ab initio* calculated VRT levels. In the  $938 \text{ cm}^{-1}$  region, they are defined with respect to the  $\Pi_{s/a, \text{lower}}(j=1, k=1)$  state. In the  $970\text{-}974 \text{ cm}^{-1}$  region, they are defined with respect to the highest  $\Pi_{s/a, \text{upper}}(j=1, k=1)$  state. As discussed in the text, there are two  $\Pi_{s/a, \text{upper}}(j=1, k=1)$  states with the same symmetry and the same approximate quantum numbers, but different in energy and with different umbrella inversion wave functions.

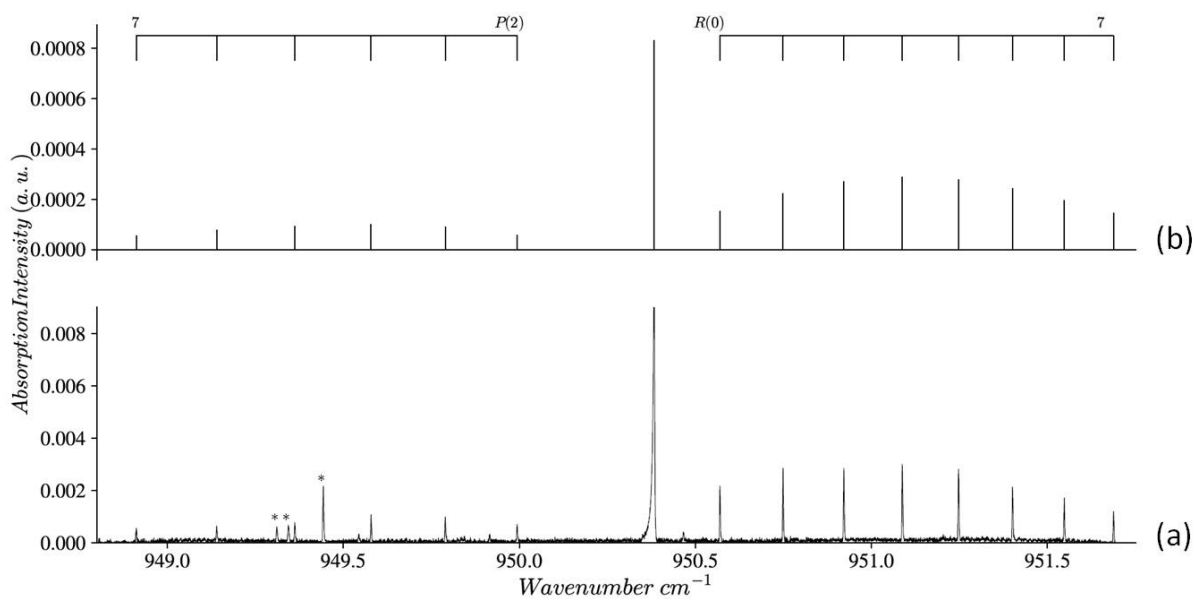


Figure 2: Jet-cooled laser spectrum of the transition  $\Pi_s(j=1, k=0) \leftarrow \Sigma_a(j=0, k=0)$  in ortho  $\text{NH}_3\text{-Ar}$  (a) compared to the PGOPHER fit of 25 rotational lines, 18  $P(J)$  and  $R(J)$  lines from the present study and 7  $Q(J)$  lines from Fraser et al.<sup>13</sup> (b). The lines marked by an asterisk are from the  $\text{NH}_3$  monomer.

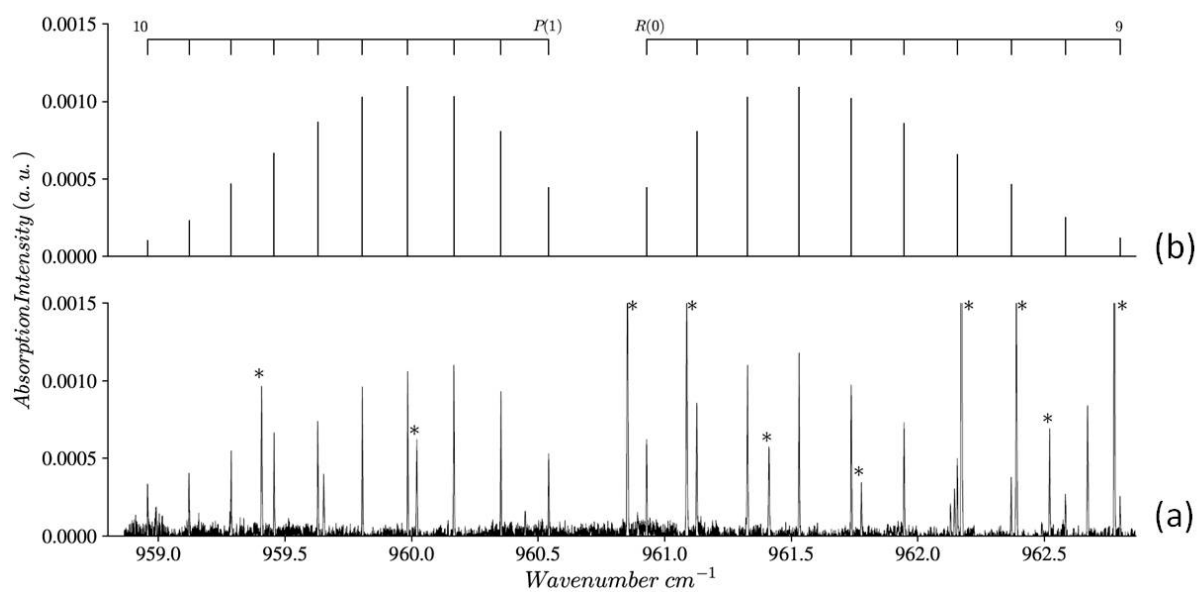


Figure 3: Jet-cooled laser spectrum of the transition  $\Sigma_s(j=1,k=0) \leftarrow \Sigma_a(j,k=0)$  in ortho  $\text{NH}_3\text{-Ar}$  (a) compared to the PGOPHER fit of 23 rotational lines observed in the present study (b). The lines marked by an asterisk are from  $\text{NH}_3$  monomer.

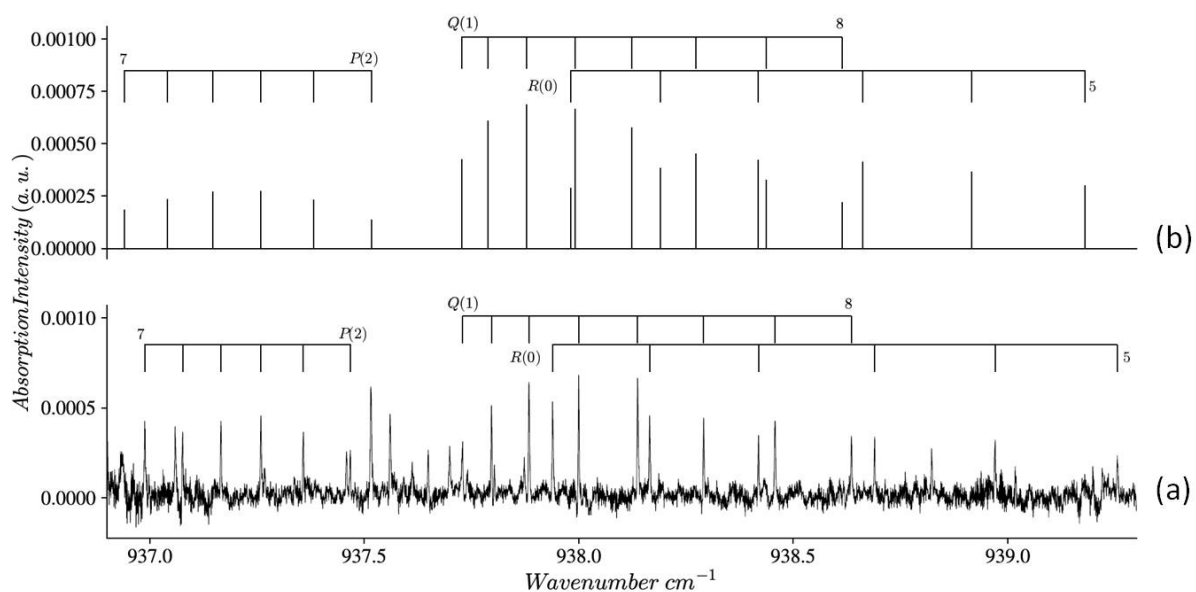


Figure 4: Jet-cooled laser spectrum of the transition  $\Pi_{s/a,lower}(j=1,k=1) \leftarrow \Sigma_a(j=1,k=1)$  in para  $\text{NH}_3\text{-Ar}$  (a) compared to the theoretical spectrum of the same transition at a rotational temperature of 3K generated with our VRT levels and transition line strengths. (b) For the sake of comparison between the spectra, the Q branch has been shifted by  $-0.12 \text{ cm}^{-1}$ , the P and R branches by  $+0.02 \text{ cm}^{-1}$  in the theoretical spectrum. The final state of the Q branch transition is  $\Pi_s$  (opposite parity with respect to  $\Sigma_a$ ), while that of the P and R branches is  $\Pi_a$  (the same parity as  $\Sigma_a$ ).

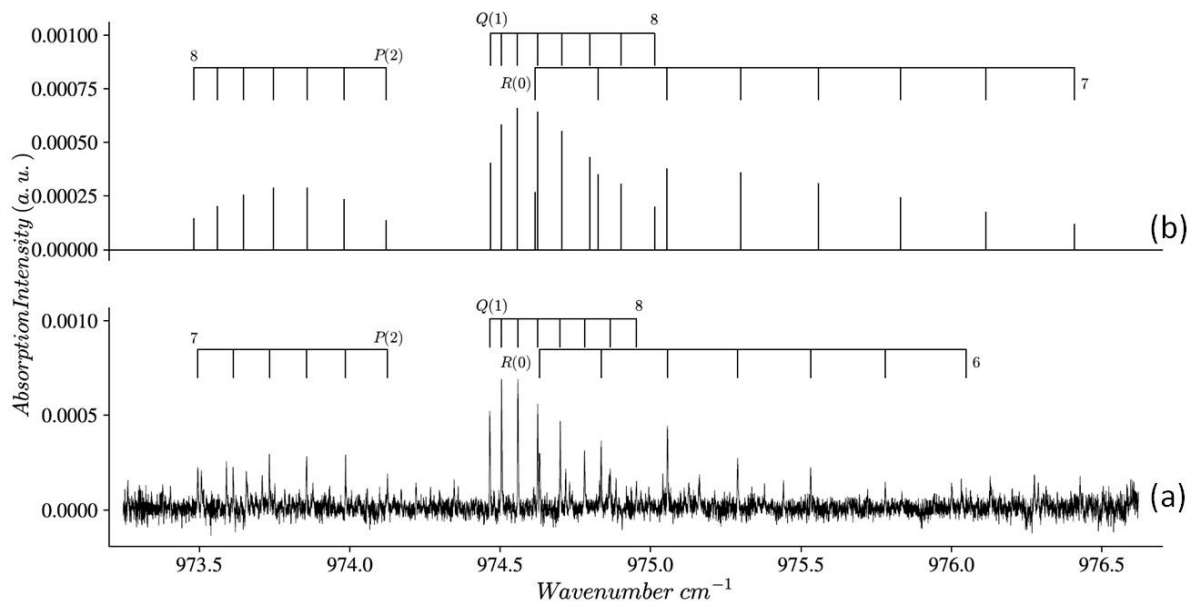


Figure 5: Jet-cooled laser spectrum of the highest transition  $\Pi_{s/a,upper}(j=1,k=1) \leftarrow \Sigma_s(j=1,k=1)$  in para  $NH_3$ -Ar (a) compared to the theoretical spectrum of the same transition at a rotational temperature of 3 K generated with our VRT levels and transition line strengths. (b) For the sake of comparison between the spectra, the theoretical spectrum has been shifted by  $+0.38 \text{ cm}^{-1}$ . The final state of the Q branch transition is  $\Pi_a$  (opposite parity with respect to  $\Sigma_s$ ), while that one of the P and R branches is  $\Pi_s$  (the same parity as  $\Sigma_s$ ).

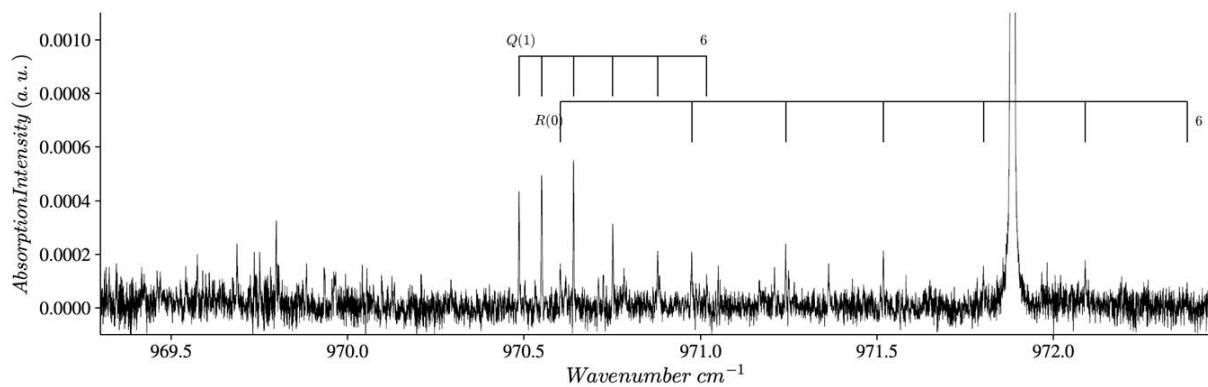


Figure 6: Jet-cooled laser spectrum of the lowest  $\Pi_{s/a,upper}(j=1,k=1) \leftarrow \Sigma_s(j=1,k=1)$  transition in para  $\text{NH}_3\text{-Ar}$ . The final state of the Q branch transition is  $\Pi_a$  (opposite parity with respect to  $\Sigma_s$ ), while that of the P and R branches is  $\Pi_s$  (the same parity as  $\Sigma_s$ ). The very intense band at  $971.88203 \text{ cm}^{-1}$  is the R(1,1) line of  $\text{NH}_3$  monomer.

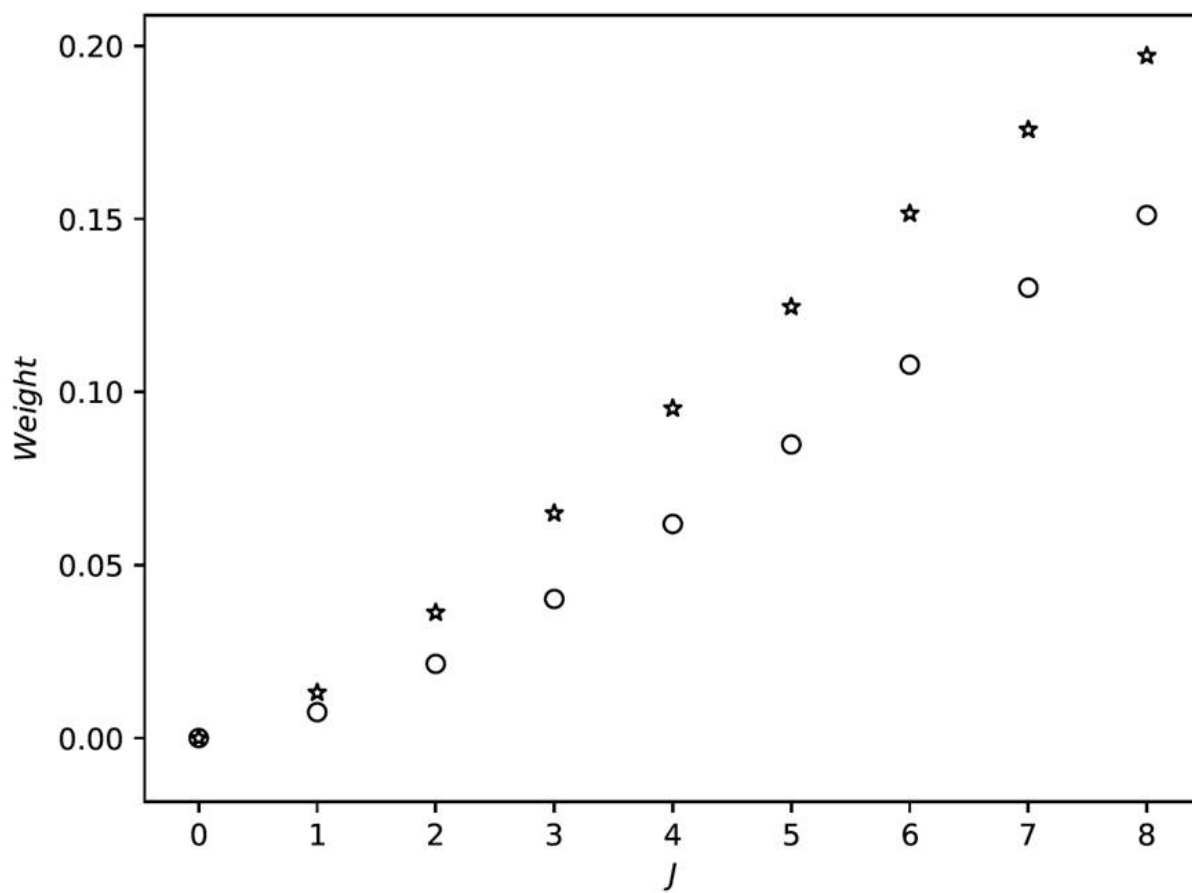


Figure 7: Relative weights of the  $\Sigma_s(j=1, k=1)$  (\*) and  $\Sigma_a(j=1, k=1)$  (o) components in the  $\Pi_{s/a}(j=1, k=1)$  ground state of para  $\text{NH}_3\text{-Ar}$ .

Transition	$\Pi_s(j=1,k=0) \leftarrow \Sigma_a(j=0,k=0)$		$\Sigma_s(j=1,k=0) \leftarrow \Sigma_a(j,k=0)$	
	Experimental	Calculated	Experimental	Calculated
P(1)	-	-	960.5416	961.285
P(2)	949.9938	949.956	960.3530	961.096
P(3)	949.7896	949.754	960.1673	960.910
P(4)	949.5789	949.547	959.9850	960.726
P(5)	949.3624	949.335	959.8056	960.545
P(6)	949.1404	949.117	959.6296	960.364
P(7)	948.9121	948.894	959.4570	960.187
P(8)	-	-	959.2873	960.012
P(9)	-	-	959.1212	959.840
P(10)	-	-	958.9574	959.668
R(0)	950.5697	950.528	960.9287	961.668
R(1)	950.7489	950.707	961.1267	961.863
R(2)	950.9216	950.880	961.3273	962.059
R(3)	951.0876	951.048	961.5310	962.258
R(4)	951.2475	951.210	961.7369	962.457
R(5)	951.4007	951.366	961.9456	962.659
R(6)	951.5476	951.516	962.1562	962.861
R(7)	951.6878	951.660	962.3689	963.065
R(8)	-	-	962.5831	963.269
R(9)	-	-	962.7992	963.475

Table 1 Experimental and *ab initio* calculated frequencies of observed transitions (in  $\text{cm}^{-1}$ ) for the  $\Pi_s(j=1,k=0) \leftarrow \Sigma_a(j=0,k=0)$  and  $\Sigma_s(j=1,k=0) \leftarrow \Sigma_a(j,k=0)$  bands of ortho  $\text{NH}_3\text{-Ar}$  complexes.

Transition	$\Pi_{s/a,lower}(j=1,k=1) \leftarrow \Sigma_a(j=1,k=1)$		$\Pi_{s/a,upper}(j=1,k=1) \leftarrow \Sigma_s(j=1,k=1)$		$\Pi_{s/a,upper}(j=1,k=1) \leftarrow \Sigma_s(j=1,k=1)$	
	Experimental	Calculated	Experimental	Calculated	Experimental	Calculated
P(2)	937.4678	937.496	974.1255	973.741	-	970.257
P(3)	937.3582	937.361	973.9862	973.602	-	970.056
P(4)	937.2592	937.238	973.8573	973.478	-	969.868
P(5)	937.1658	937.126	973.7332	973.367	-	969.695
P(6)	937.0770	937.020	973.6127	973.268	-	969.538
P(7)	936.9882	936.920	973.4949	973.180	-	969.393
Q(1)	937.7294	937.847	974.4658	974.088	970.4858	970.602
Q(2)	937.7967	937.909	974.5048	974.124	970.5501	970.571
Q(3)	937.8841	937.999	974.5594	974.177	970.6406	970.546
Q(4)	937.9998	938.111	974.6250	974.245	970.7514	970.525
Q(5)	938.1371	938.244	974.6998	974.325	970.8790	970.507
Q(6)	938.2911	938.393	974.7808	974.419	971.0173	970.488
Q(7)	938.4576	938.557	974.8658	974.521	-	970.464
Q(8)	938.6356	938.734	974.9533	974.634	-	970.432
R(0)	937.9391	938.004	974.6304	974.261	970.6029	970.777
R(1)	938.1652	938.213	974.8362	974.471	970.9757	970.925
R(2)	938.4191	938.441	975.0561	974.699	971.2413	971.089
R(3)	938.6896	938.684	975.2893	974.944	971.5181	971.272
R(4)	938.9709	938.938	975.5321	975.203	971.8019	971.472
R(5)	939.2555	939.202	975.7803	975.476	972.0899	971.689
R(6)	-	-	976.0490	975.760	972.3789	971.918

Table 2: Experimental and *ab initio* calculated frequencies of observed transitions (in  $\text{cm}^{-1}$ ) for the  $\Pi_{s/a,lower}(j=1,k=1) \leftarrow \Sigma_a(j=1,k=1)$  and for both  $\Pi_{s/a,upper}(j=1,k=1) \leftarrow \Sigma_s(j=1,k=1)$  bands of para  $\text{NH}_3\text{-Ar}$  complexes.

	$\Sigma_a(j=0,k=0)$	$\Pi_s(j=1,k=0)$		$\Sigma_s(j=1,k=0)$ This work Calculated
		This work Calculated	Fraser et al.	
$\nu_0$ (cm <sup>-1</sup> )		950.38396(7) 950.342(3)	950.38769(3)	960.73361(5) 961.475(3)
$B''(B')$ (MHz)	2876.84901(79)	2826.06(43) 2837.6(84)	2826.9116(93)	2922.83(5) 2913.0(80)
$D_J''(D_J')$ (MHz)	0.088695(98)	0.07276(52) 0.18(11)	0.07815(19)	0.11470(33) 0.22(12)
$q'$ (MHz)		88.46(81) 81.5(88)	90.928(12)	
Number of lines		19	18	23
RMS error (MHz)		4.3	0.25	5.0

Table 3: Molecular parameters for the transitions  $\nu_2=1\leftarrow 0$   $\Pi_s(j=1,k=0)\leftarrow \Sigma_a(j,k=0)$  and  $\Sigma_s(j=1,k=0)\leftarrow \Sigma_a(j,k=0)$  of ortho NH<sub>3</sub>-Ar. The molecular parameters of the  $\Sigma_a(j,k=0)$  state are given by Nelson et al.<sup>4</sup> For the  $\Pi_s(j=1,k=0)$  state, the molecular parameters reported in the column “this work” are obtained from a line list composed of 18 P( $J$ ) and R( $J$ ) rotational lines observed by direct absorption spectroscopy (this work) supplemented with 7 Q( $J$ ) lines observed using saturated absorption spectroscopy by Fraser et al.<sup>13</sup> This set of parameters is compared to that obtained by Fraser et al.<sup>13</sup> with a resolution twenty times better. The parameters “calculated” are from fits to the VRT levels calculated for  $J$  values up to 10.

Transition	$\nu_0$ (cm <sup>-1</sup> ) exp	$\nu_0$ (cm <sup>-1</sup> ) calc
$\Pi_s(j=1,k=0)\leftarrow \Sigma_a(j=0,k=0)$	950.38396(7)	950.342(5)
$\Sigma_s(j=1,k=0)\leftarrow \Sigma_a(j,k=0)$	960.73361(3)	961.475(3)
$\Pi_{s/a,lower}(j=1,k=1)\leftarrow \Sigma_a(j=1,k=1)$	937.6621*	937.7821*
$\Pi_{s/a,upper}(j=1,k=1)\leftarrow \Sigma_s(j=1,k=1)$	970.4220*	970.6340*
$\Pi_{s/a,upper}(j=1,k=1)\leftarrow \Sigma_s(j=1,k=1)$	974.4268*	974.0468*

Table 4: Experimental and calculated band origins of the observed bands. The asterisk \* marks the band origins of para bands corresponding to the extrapolated Q(0) rotational line.

## References

---

- <sup>1</sup> F. Pirani, L. Roncaratti, L. Belpassi, F. Tarantelli, and D. Cappelletti, *J. Chem. Phys.* **135**, 194301 (2011).
- <sup>2</sup> D. D. Nelson, Jr., G. T. Fraser, and W. Klemperer, *Science* **238**, 1670 (1987).
- <sup>3</sup> G. Fraser, D. Nelson, Jr., A. Charo, and W. Klemperer, *J. Chem. Phys.* **82**, 2535 (1985).
- <sup>4</sup> D. Nelson, Jr., G. Fraser, K. I. Peterson, K. Zhao, and W. Klemperer, *J. Chem. Phys.* **85**, 5512 (1986).
- <sup>5</sup> E. Zwart and W. Meerts, *Chem. Phys.* **151**, 407 (1991).
- <sup>6</sup> C. Schmuttenmaer, R. Cohen, J. Loeser, and R. Saykally, *J. Chem. Phys.* **95**, 9 (1991).
- <sup>7</sup> C. Schmuttenmaer, J. Loeser, and R. Saykally, *J. Chem. Phys.* **101**, 139 (1994).
- <sup>8</sup> E. Zwart, H. Linnartz, W. Meerts, G. Fraser, D. Nelson, Jr., and W. Klemperer, *J. Chem. Phys.* **95**, 793 (1991).
- <sup>9</sup> A. Grushow, W. Burns, S. Reeve, M. Dvorak, and K. Leopold, *J. Chem. Phys.* **100**, 2413 (1994).
- <sup>10</sup> C. A. Schmuttenmaer, R. C. Cohen, and R. J. Saykally, *J. Chem. Phys.* **101**, 146 (1994).
- <sup>11</sup> G. Bistoni, L. Belpassi, F. Tarantelli, F. Pirani, and D. Cappelletti, *J. Phys. Chem. A* **115**, 14657 (2011).
- <sup>12</sup> J. Loreau, J. Liévin, Y. Scribano and A. van der Avoird, *J. Chem. Phys.* **141**, 224303 (2014).
- <sup>13</sup> G. T. Fraser, A. S. Pine, and W. A. Kreiner, *J. Chem. Phys.* **94**, 7061 (1991).
- <sup>14</sup> A. Bizzari, B. Heijman, S. Stolte, and J. Reuss, *Z. Phys. D* **10**, 291 (1988).
- <sup>15</sup> K. Didriche, T. Földes, T. Vanfleteren, and M. Herman, *J. Chem. Phys.* **138**, 181101 (2013).
- <sup>16</sup> J. Loreau and A. van der Avoird, *J. Chem. Phys.* **143**, 184303 (2015).
- <sup>17</sup> O. Tkac, A. K. Saha, J. Loreau, D. H. Parker, A. van der Avoird, and A. J. Orr-Ewing, *J. Phys. Chem. A* **119**, 5979 (2015).
- <sup>18</sup> A. P. P. van der Poel, P. C. Zieger, S. Y. T. van de Meerakker, J. Loreau, A. van der Avoird, and H. L. Bethlem, *Phys. Rev. Lett.* **120**, 033402 (2018).
- <sup>19</sup> G. Brocks, A. van der Avoird, B. T. Sutcliffe, and J. Tennyson, *Mol. Phys.* **50**, 1025 (1983).
- <sup>20</sup> A. van der Avoird, P. E. S. Wormer, and R. Moszynski, *Chem. Rev.* **94**, 1931 (1994).
- <sup>21</sup> J. van Bladel, A. van der Avoird, and P. Wormer, *Chem. Phys.* **165**, 47 (1992).
- <sup>22</sup> K. B. Gubbels, S. Y. T. van de Meerakker, G. C. Groenenboom, G. Meijer, and A. van der Avoird, *J. Chem. Phys.* **136**, 074301 (2012).
- <sup>23</sup> E. H. T. Olthof, A. van der Avoird, and P. E. S. Wormer, *J. Chem. Phys.* **101**, 8430 (1994).
- <sup>24</sup> G. C. Groenenboom, P. E. S. Wormer, A. van der Avoird, E. M. Mas, R. Bukowski, and K. Szalewicz, *J. Chem. Phys.* **113**, 6702 (2000).
- <sup>25</sup> A. van der Avoird and D. Nesbitt, *J. Chem. Phys.* **134**, 044314 (2011).
- <sup>26</sup> M. P. Ziemkiewicz, C. Pluetzer, M. Wojcik, J. Loreau, A. van der Avoird, and D. J. Nesbitt, *J. Chem. Phys.* **146**, 104204 (2017).
- <sup>27</sup> M. P. Ziemkiewicz, C. Pluetzer, J. Loreau, A. van der Avoird, and D. J. Nesbitt, *J. Chem. Phys.* **147**, 214304 (2017).
- <sup>28</sup> D. T. Colbert and W. H. Miller, *J. Chem. Phys.* **96**, 1982 (1992).
- <sup>29</sup> G. C. Groenenboom and D. T. Colbert, *J. Chem. Phys.* **99**, 9681 (1993).
- <sup>30</sup> E. Davidson, *J. Comput. Phys.* **17**, 87 (1975).
- <sup>31</sup> M. P. Ziemkiewicz, C. Pluetzer, D. J. Nesbitt, Y. Scribano, A. Faure, and A. van der Avoird, *J. Chem. Phys.* **137**, 084301 (2012).

- 
- <sup>32</sup> P. Asselin, Y. Berger, T. R. Huet, R. Motiyenko, L. Margulès, R. J. Hendricks, M. R. Tarbutt, S. Tokunaga, B. Darquié, *Phys. Chem. Chem. Phys.* **19**, 4576 (2017).
- <sup>33</sup> P. Asselin, A. Potapov, A. C. Turner, V. Boudon, L. Bruel, M-A. Gaveau, M. Mons, *Phys. Chem. Chem. Phys.* **19**, 17224 (2017).
- <sup>34</sup> M. D. Brookes, C. Xia, J. A. Anstey, B. G. Fulsom, K.-X. Au Yong, J. M. King and A. R. W. McKellar, *Spectrochim. Acta, Part A*, **60**, 3235 (2004).
- <sup>35</sup> L.S. Rothman, I.E. Gordon, Y. Babikov, A. Barbe, D. C Benner, P.F. Bernath, M. Birk, L. Bizzocchi, V. Boudon, L.R. Brown, A. Campargue, K. Chance, E.A. Cohen, L.H. Coudert, V.M. Devi, B.J. Drouin, A. Fayt, J.-M. Flaud, R.R. Gamache, J.J. Harrison, J.-M. Hartmann, C. Hill, J.T. Hodges, D. Jacquemart, A. Jolly, J. Lamouroux, R.J. Le Roy, G. Li, D.A. Long, O.M. Lyulin, C.J. Mackie, S.T. Massie, S. Mikhailenko, H.S.P. Müller, O.V. Naumenko, A.V. Nikitin, J. Orphal, V. Perevalov, A. Perrin, E.R. Polovtseva, C. Richard, M.A.H. Smith, E. Starikova, K. Sung, S. Tashkun, J. Tennyson, G.C. Toon, Vl.G. Tyuterev, G. Wagner, *JQSRT*, **130**, 4 (2013).
- <sup>37</sup> P. Bernath, *Spectra of atoms and molecules*, pp249-250, New York, Oxford University press (1995).
- <sup>38</sup> M. P. Ziemkiewicz, C. Pluetzer, D. J. Nesbitt, Y. Scribano, A. Faure and A van der Avoird, *J. Chem. Phys.* **137**, 084301 (2012).
- <sup>39</sup> T. Vanfleteren, T. Foldes, M. Herman, J. Liévin, J. Loreau, and L. Coudert, *J. Chem. Phys.* **147**, 014302 (2017).